Single Crystals of Polythiophene with Different Molecular Conformations Obtained by Tetrahydrofuran Vapor Annealing and Controlling Solvent Evaporation

Xinli Xiao, Zongbao Wang,[‡] Zhijun Hu,[§] and Tianbai He*[,†]

State Key Laboratory of Polymer Physics and Chemistry, Changchun Institute of Applied Chemistry, Chinese Academy of Sciences, Changchun, 130022, P. R. China, Ningbo Key Laboratory of Polymer Materials, Ningbo Institute of Material Technology and Engineering, Chinese Academy of Sciences, Ningbo, 315201, P. R. China, and Center for Soft Condensed Matter Physics and Interdisciplinary Research, Soochow University, Suzhou, 215006, P. R. China

Received: December 04, 2009; Revised Manuscript Received: March 29, 2010

Single crystals of poly(3-hexylthiophene) (P3HT) and poly(3-octylthiophene) (P3OT) have been prepared by tetrahydrofuran vapor annealing and controlling solvent evaporation, respectively. The morphology and structure of the single crystals are characterized using optical microscopy, scanning electron microscopy, atomic force microscopy, transmission electron microscopy, and wide-angle X-ray diffraction. It is observed that in P3HT single crystals, the molecules are packed with $\pi-\pi$ stacking direction perpendicular to the length axis of the crystals and main chains parallel to the substrate, whereas in P3OT single crystals, the molecules are packed with $\pi-\pi$ stacking direction parallel to the length axis of the crystal and main chains parallel to the substrate. In the field effect transistors, the current flow is parallel to the length axis of the single crystals, and the mobility is 1.57×10^{-3} cm^2/Vs for a P3HT single crystal and 0.62 cm^2/Vs for a P3OT single crystal. The single crystals of P3HT and P3OT showed high anisotropic electrical properties. The influences of molecular conformation and alkyl chain length on the electrical properties of P3ATs are discussed.

1. Introduction

Poly(3-alkylthiophene)s (P3ATs) have been the focus of many studies from both scientific and industrial areas due to their solubility and high mobility.[1−25] Extensive efforts have been carried out to correlate the P3AT structures with the device performances because a fundamental understanding of the structure−property relationships is of vital importance to device applications.[7,16−25] To link structures with properties, it is necessary that variations in microstructure and overall molecular ordering are minimized or eliminated. However, many physical studies are performed on P3AT polycrystalline films containing structure mixtures and defects, which may lead to difficulties in data interpretation and even incorrect conclusions.[16−25]

The intrinsic anisotropy of conducting polymers at the molecular level can lead to anisotropy in terms of macroscopic properties, such as charge transport and photoluminescence (PL) emissions.[26−28] The apprehension of anisotropy is useful in improving the stability and conductivity of a conducting polymer, which are the key factors in determining device performance.[29] Nevertheless, the common polycrystalline P3AT films prepared without using a polymer arrangement technique exhibit in-plane isotropic properties. It has been proved that the molecular conformation is the most crucial parameter of controlling the charge transport and anisotropy of the conjugated polymer films.[29−37] The field-effect transistor (FET) based on organic molecular single crystals has exhibited a high anisotropy of electrical properties with respect to the molecular conformations.[25,26,38] Therefore, a better and more detailed analysis of the anisotropic structure−property relationships of P3ATs is expected to be obtained from single crystals with specific molecular conformation and perfect molecular ordering. Although single crystals of different P3ATs with different molecular conformations have shown different electrical properties,[35−37] single crystals of the same sample with different molecular conformations are expected to provide more convincing evidence for the anisotropic molecular conformation−charge transport studies.

The alkyl side chains play an important role in the electrical properties of P3ATs, and yet, accurate knowledge of the dependence of mobility on the alkyl side length is still lacking.[39−43] As in a polycrystalline film, mobility is a function of not only the alkyl chain length but also other variables, such as the degree of crystallinity, crystallite size, etc.[42,43] As a result,single crystals of different P3ATs with the same molecular conformation are expected to further clarify the alkyl chain length-electrical property relationships due to the negligible morphological variables and impurities in single crystals.

Among the P3ATs, poly(3-hexylthiophene) (P3HT) is the most widely used, followed by poly(3-octylthiophene) (P3OT). Therefore, single crystals of P3HT and P3OT are preferred as the candidates for the structure−electrical property analysis of P3ATs in our study. Single crystals of P3HT with the $\pi-\pi$ stacking direction parallel to the length axis of the crystal and P3OT with the $\pi-\pi$ stacking direction perpendicular to the length axis of the crystal have been reported.[35,37] Here, we demonstrate that single crystals of P3HT with the $\pi-\pi$ stacking direction perpendicular to the length axis of the crystal can be obtained by tetrahydrofuran (THF) vapor annealing, and single crystals of P3OT with the $\pi-\pi$ stacking direction parallel to the length axis of the crystal can be obtained by controlling solvent evaporation. The effects of molecular conformation and alkyl chain length on the electrical properties of the P3HT and P3OT single crystals are discussed, and these results may

* To whom correspondence should be addressed. Phone: +86-431-85262123. Fax: +86-431-85262126. E-mail: tbhe@ciac.jl.cn.
‡ Ningbo Institute of Material Technology and Engineering.
§ Soochow University.
† Changchun Institute of Applied Chemistry.

10.1021/jp911525d
Published on Web 05/17/2010

contribute to further structure−property study of conjugated polymers as well as future device applications.

2. Experimental Section

2.1. Materials. Regioregular P3HT and P3OT samples with a given regioregularity of 98.5% were purchased from Aldrich, and the polymers were purified by continuous extraction with THF and acetonitrile of high-pressure liquid chromatography grade. The weight-average molecular weight and polydispersity index were measured as 3.96×10^4 g mol^{-1} and 1.92 for P3HT and 5.12×10^4 g mol^{-1} and 1.86 for P3OT. Chloroform was purchased from Beijing Chemical Works, and THF and chlorobenzene were purchased from Sinopharm Chemical Reagent Co. Ltd. Carbon fiber with a diameter of 2.6 mm was purchased from Ted Pella, Inc. Heavily doped silicon wafer with a 144-nm-thick SiO_2 layer was used as substrate.

2.2. Preparations. ***2.2.1. Preparation of P3HT Single Crystals.*** The P3HT sample was dissolved in chloroform at a concentration of 0.06% (w/v). The substrate was put inside a cylinder container with a radius and height of 1.5 and 3.0 cm, respectively. A drop of solution was deposited onto the substrate, and the container was then covered with a lid, and a polycrystalline film was obtained after the solvent evaporated. THF vapor annealing was carried out by placing an open container full of THF beneath the film in an airtight container at 35 °C under ambient pressure. After annealing, the samples were maintained under vacuum at 60 °C for 48 h to remove the residual solvent before measurement.

2.2.2. Preparation of P3OT Single Crystals. The P3OT sample was dissolved in chlorobenzene at a concentration of 0.04% (w/v), and a drop of solution was deposited onto the substrate. A slow solvent evaporation rate was achieved by placing the solution-cast films inside a cylinder container with a radius and height of 2.0 and 3.0 cm, respectively, covered with a lid. Chlorobenzene drops were deposited around the substrate to generate a chlorobenzene partial pressure. Under these conditions, solvent can escape only through the small gap between the container and its lid. The solvent in solution and the container evaporated completely at 20 °C after about 100 h.

2.3. Characterizations. The optical microscopy and scanning electron microscopy (SEM) images were obtained using a Leica DMLP and FEL XL 30, respectively. The height of the crystals was studied by atomic force microscopy (AFM) performed on a SPA 300HV instrument with an SPI 3800N controller (Seiko Instruments Industry Co., Ltd.) at room temperature in air. The images were obtained by means of the tapping mode (height and phase) with a silicon nitride cantilever (Olympus Optical Co. Ltd., Tokyo, Japan) having a spring constant of 42 N/m and a resonating frequency of 300k Hz, and the scanning rates varied from 0.5 to 1 Hz. For transmission electron microscopy (TEM) examination, an ~20 nm amorphous carbon film was evaporated onto the above-mentioned silicon wafer, and the carbon-coated silicon wafer was used as the substrate. The samples for TEM were floated away from the substrate in hydrofluoric solution and then transferred to a copper grid. A respirator, safety glasses, disposable latex gloves, and lab gown are necessary when handling the hydrofluoric solution, and great care must be employed during this process. TEM experiments were performed using a JEOL JEM-1011 with an accelerating voltage of 100 kV for bright field TEM and selected area electron diffraction (SAED) modes. The camera length was calibrated with Au to calculate the *d*-spacing of the observed electron diffractions. The X-ray diffraction (XRD) patterns were obtained using a Bruker D8 Discover Reflector with X-ray generation power of 40 kV tube voltages and 40 mA tube current. XRD patterns were taken in reflection mode in the 2θ range from 2 to 30° by continuous scanning with a step size of 0.04°. The same process to make FET reported previously was employed here, and the heavily doped silicon wafer was used as the substrate as well as the gate. The thermally grown 144 nm SiO_2 layer functions as the gate dielectric layer.[37] Source-drain electrodes (Au) were evaporated through a shadow mask onto the crystal. The current−voltage ($I-V$) characteristics of the FET based on the single crystals were measured by using a Keithley 237, a high-voltage source-measurement unit, at room temperature.

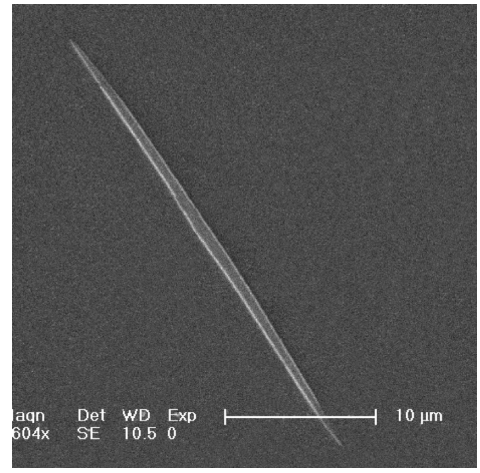

Figure 1. SEM image of a typical P3HT single crystal obtained by THF vapor annealing.

3. Results and Discussions

3.1. P3HT Single Crystals Obtained by THF Vapor Annealing. ***3.1.1. Morphology and Structure Analysis of P3HT Single Crystals.*** The P3HT single crystals are mainly needlelike crystals with a length of 20−60 μm and a diameter of 1−2.2 μm when the film has been annealed for 42 h. The SEM image of a typical crystal is shown in Figure 1. The P3HT single crystals are much like the needlelike crystals simulated by the phase-field theory without foreign particles or frozen-in orientation defects;[44] the optical and SEM images of the crystals with different sizes are shown in the Supporting Information (Figures S1 and S2, respectively). The crystals possess a height of several hundred nanometers and the height shows a gradual decrease toward the tip. The AFM height image of a typical crystal with the detailed analysis of its height is shown in Supporting Information Figure S3. It is observed that in the morphology, the P3HT single crystals are similar to the P3OT single crystals obtained by the same process, as well as the needlelike whiskers of poly(oxy-1,4-benzenediylcarbonyl), poly(4-hydroxybenzoate), and polyoxymethylene prepared by polycondensation of monomers in solution.[37,45−47]

The structures of P3ATs have been studied extensively, and many different results have been derived, depending on the monomer unit, the polymerization method, the molecular weight, the film-processing conditions, and so on.[3,16,17,34,48−50] It is generally considered that the crystalline portions of P3AT consist of stacked polymer chains, and we denote the separation of the main chain stacks as the *a* axis, the repetition distance along $\pi-\pi$ stacking direction of the main chains as the *b* axis, and the repetition distance along the polymer chains as the *c* axis according to the common usage.[41,51]

Polymorphic behaviors have been observed in P3ATs, and it is suggested that the side chain interdigitation is minimal in

the more common phase 1. A side-by-side arrangement is typical of this phase, whereas the side chain interdigitation is prevalent in phase 2.[50,52−54] According to the calculations from the ideal model, in which the side chains are fully extended with both the main chains and the side chains adopting an all-trans-planar conformation, the *d*-spacing of the *a* axis is 17.4 Å for PHT.[12] As a matter of fact, the values of *a* are reported to be around 16.0 Å in most cases, and P3HT crystallized in this form is assigned as phase 1, whereas P3HT crystallized with *a* around 12.0 Å is assigned as phase 2.[18,34,52] The experimentally observed *a* of phase 1 for P3HT varied from about 15.5 to about 17.3 Å, depending on the molecular weights and processions.[3,12,34,52]

The XRD results of many reports indicate that strictly speaking, interdigitation of the alkyl side chains exists in both phases 1 and 2 of P3ATs, and the difference in the two phases lies mainly in the extent of interdigitation.[51,56,57] The minimal interdigitation of alkyl side chains in phase 1 could provide extra stabilization of the fully planar conformation and the crystalline structure due to the so-called "zipper effect"; the crowding of alkyl chains caused by the much higher extent of interdigitation may be the main factor that rendered phase 2 a metastable polymorph.[56,57] It has been observed that in both polymorphs of P3ATs, *a* increased with the elongation of the alkyl side chain length in an essentially linear relationship, and *c* is universally accepted as the repetition distance along the polythiophene main chains.[16,51,53]

However, the $\pi-\pi$ stacking distance of P3ATs appears to differ from materials without regular progression. For P3ATs in phase 1, the $\pi-\pi$ stacking distance in many cases is reported to be about 3.7−3.9 Å,[7,51,54] whereas a much larger distance of 4.85 Å was reported for P3OT.[55] For P3ATs in phase 2, the $\pi-\pi$ stacking distance is considered to be larger than that of phase 1: the distance was reported to be 4.47, 4.7, 5.2, or 5.5 Å under different conditions,[48,53−55,58] and an unusually large separation (>7 Å) was even reported for poly(3-decylthiophene) (P3DT).[59] Despite the directly obtained experimental results, the possible models for P3ATs that correspond to the energetically most stable structures and yield the best agreement between simulated and experimental fiber patterns have been proposed. One structure for P3HT was phase 1 with a $\pi-\pi$ stacking distance of 4.14 Å, and a similar structure for P3DT was phase 1 with a $\pi-\pi$ stacking distance of 4.13 Å.[50]

The crystal structure and molecular conformation of the P3HT single crystals obtained by THF vapor annealing are characterized with XRD and SAED patterns. The out-of-plane XRD profiles of the crystals grown on a silicon wafer are shown in Figure 2a, and the *d*-spacing of 16.36 Å with a series of (h00) reflections as (100), (200), and (300) are observed. The XRD results indicate that P3HT crystallizes preferentially in phase 1 under THF vapor annealing and the experimental value deviates from the calculated value by 1.04 Å, confirming the minor interdigitation of alkyl side chains in phase 1.[12,56] The XRD results also suggest that the *a* axis is oriented perpendicular to the crystal surface with the *bc* plane of the crystal on the substrate, the same as the molecular conformation of P3OT single crystals obtained by THF vapor annealing.[37]

The TEM image and the corresponding SAED of the crystal are shown in Figure 2b and c, respectively. A repetition unit of 7.42 Å along the polymer chain direction and a repetition unit of 8.38 Å along the $\pi-\pi$ stacking direction are observed from the SAED results.[16,37,50] The $\pi-\pi$ stacking distance of 4.19 Å in the P3HT single crystals is consistent with the value of 4.14 Å for the energetically most stable structure in phase 1with a negligible deviation of 0.05 Å but deviates from the $\pi-\pi$ stacking distance of phase 2 (4.47 Å, 4.7 Å, 5.2 Å, et al.) greatly.[50,53−55] It can then be inferred that the phase 1structure with the obtained cell parameters is the thermostable form for P3HT single crystals under THF-vapor annealing. It is observed that high molecular weight and high regioregularity favored phase I of P3ATs, whereas the regioirregular low-molecular-weight systems tend to crystallize preferentially in phase 2.[52,53]

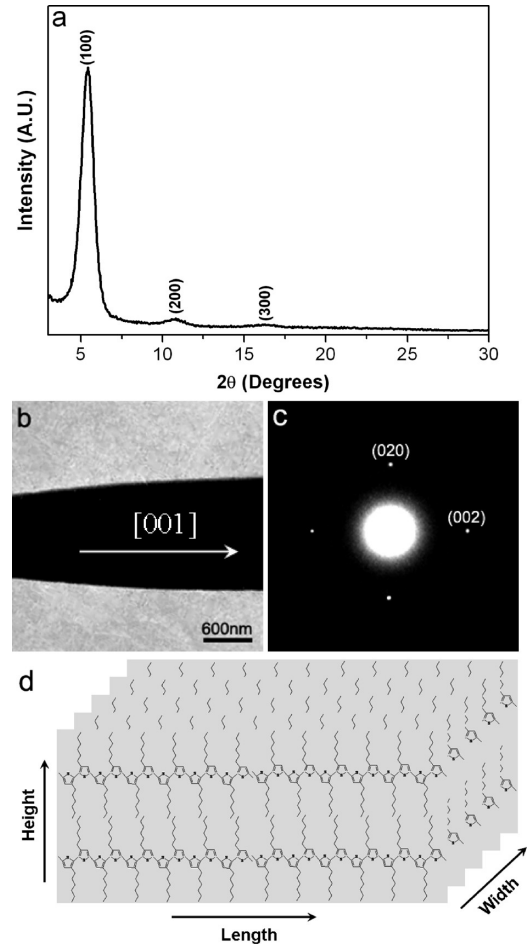

Figure 2. Structure and molecular conformation of the P3HT single crystals. (a) XRD profiles of P3HT crystals grown on a silicon wafer. (b) TEM image of part of a single crystal. (c) SAED pattern obtained perpendicular to the length axis of the crystal. (d) Schematic illustrations for the assembly of the extended polymer chains in the crystal. For clarity, the relative dimensions are not drawn to scale.

In addition to the crystallization conditions, the high molecular weight of 40k and high regioregularity of 98.5% of the P3HT used in our experiments might also contribute to the presence of phase 1. The 0*kl* reflections in SAED patterns manifest that the electron beam goes along [100] zone axis, coinciding with the (100) projection from XRD results. As far as we know, the needlelike polymer whiskers and single crystals reported until now are all composed of extended-chain molecules that are packed with the main chains parallel to the length axis of the crystal,[37,45−47,60] and the length axis of the P3HT single crystal obtained here is also observed to be along the [001] direction. From the XRD and SAED analysis, it can be deduced that the P3HT molecules in the single crystal are oriented with the $\pi-\pi$ stacking direction perpendicular to the length axis of the crystals and the main chains parallel to the substrate. The schematic illustration for the assembly of the molecules is manifested in Figure 2d.

3.1.2. Growth of P3HT Single crystals. The effects of solvent vapor annealing on many organic functional materials, including

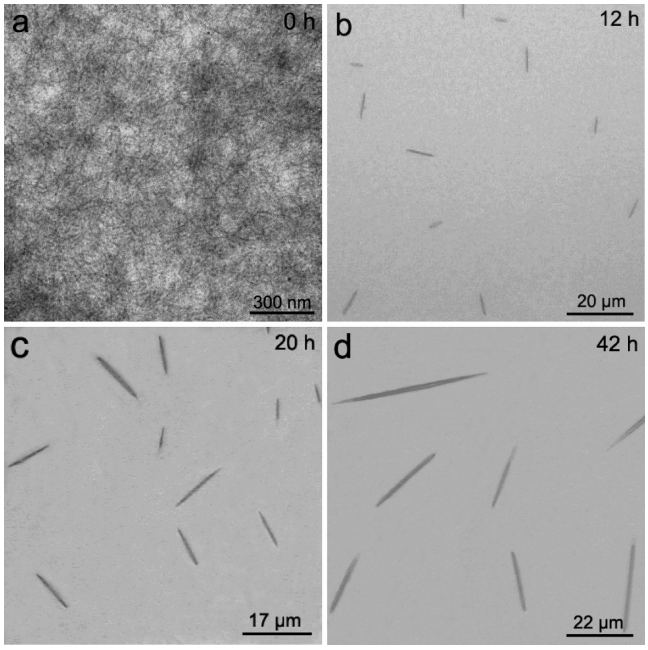

Figure 3. Time-dependent morphology of the P3HT crystals with different annealing times of 0 (a), 12 (b), 20 (c), and 42 h (d).

P3ATs, have been studied, and various results have been obtained using the different organic solvents and processing conditions.[37,58,61−67] When the film is exposed to the vapor of a solvent in which the film tended to have a low to slight solubility, the adsorption of solvent molecules during solvent vapor exposure was presumed to result in a saturated solvent solution on the film surface. The adsorbed solvent may render a relaxation of a metastable crystal lattice or an increase in molecular mobility at the surface of the film and, thus, induce the nucleation of a stable crystalline form.[58,65−67] The molecules on the crystal surface are energetically less favored than those packed in the interior; thus, the larger particles with greater volume-to-surface-area ratio have a lower solubility than the smaller ones.[68] When the film is solvent-vapor-annealed, crystals of a "critical" size have solubility equal to that of the supersaturated vapor/solution above the film surface. Thus, crystals with a size smaller than the "critical" size have a higher solubility and tend to dissolve while larger crystals will be insoluble and tend to grow. During this process, many small crystals formed initially disappeared, except for a few that grow larger at the expense of the smaller ones. In this way, the crystals undergo Ostwald ripening, similar to the ripening of precipitates in solution, and the absorbed solvent molecules act as the transport media for growth.[65,67]

The growth process of the P3HT crystals was studied. The morphologies of the crystals with different annealing time are shown in Figure 3. The P3HT solution initially formed polycrystalline film, as shown in Figure 3a, and some crystals with average lengths of ~10 μm were observed when the film had been annealed for 12 h (Figure 3b). The crystals grew to an average length of 16 and 32 μm when the annealing time was extended to 20 (Figure 3c) and 42 h (Figure 3d), respectively. As seen in the AFM height image of a crystal with a length of ~10 μm (Supporting Information Figure S4), the height of the crystal is tens of nanometers, much thinner than that of the fully grown crystals (Supporting Information Figure S3). The crystals grew larger with the increase in the annealing time within this time scale, and thus, the growth is attributed to Ostwald ripening.[65,67] Further extension of annealing time did not induce discernible change in crystal size due to the fact that the amount of residual materials decreases with the increase in the crystals, and the growth of crystals stopped when the amorphous materials were exhausted. This is consistent with the previous observations that in a solvent-vapor-annealed film, once a crystal nucleus has formed, the crystals grow until the entire amorphous layer has been transformed.[37,65,67] No amorphous zones are observed surrounding the fully grown P3HT single crystal in either the TEM or AFM images, which indicates that the crystals are not embedded in a "base film" of polythiophene that did not crystallize.

In the solution-cast RR-P3AT films, crystals are usually formed with the $\pi-\pi$ stacking direction parallel to the growth axis of the crystal and the main chains parallel to the substrate because the $\pi-\pi$ intermolecular interactions mainly determine the growth of the crystals during the solution-crystallization process.[23,35,59,69] In the friction-transferred film, the molecules are packed with the $\pi-\pi$ stacking direction perpendicular to the substrate and the main chains parallel to the drawing direction; the external effect exerted on the film was considered to cause this phenomenon.[31,70] Different from the molecular conformations in solution-cast or friction-transferred films, when the P3HT film is THF-vapor-annealed, the molecules in the single crystal are packed with the $\pi-\pi$ stacking direction perpendicular to the length axis of the crystal and the main chains parallel to the substrate. These results indicate that the crystallization conditions have a vital influence on the molecular conformations of P3ATs. For the THF-vapor-annealed P3HT film, the interaction between the P3HT molecules and the THF molecules from the saturated THF vapor can be regarded as an external effect that determines the formation and corresponding molecular conformation of the single crystals. The accurate interaction relationships between P3HT and THF molecules are under investigation, and solvent-vapor annealing experiments with other solvents and process conditions will be carried out for further studies.

3.1.3. Electrical Properties of P3HT Single Crystals. The schematic illustration for the configuration of FET base on the P3HT and P3OT single crystals, the SEM image of the crystals measured, and the detailed parameters for the FET are shown in the Supporting Information (Figure S5). The source−drain current (I_{DS}) curves versus the drain voltage (V_{DS}) with different gate voltages (V_{GS}) of the FET based on the P3HT single crystal are shown in Figure 4a. The $-I_{DS}$ increased with the increase in $-V_{GS}$, indicating a p-type output characteristic. The transfer characteristics in Figure 4b manifest the $-I_{DS}$ and $(-I_{DS})^{1/2}$ curves versus $-V_{GS}$ when V_{DS} is -15 V. As shown in Figure 4c, no channel conductance or gate dependence is detected in the FET based on the annealed film in regions without P3HT single crystals, which clearly demonstrates that the gate modulation is attributed to the P3HT single crystal between the two electrodes. The field-effect mobility of the FET is calculated in the saturation regime with eq 1,

$$I_{DS} = \frac{W}{2L}\mu C_i(V_{GS} - V_{Th})^2 \quad (1)$$

where μ is the effective mobility, W is the channel width, L is the channel length, and C_i is the capacitance of the gate insulator per unit area. An effective mobility of 1.57×10^{-3} cm^2/Vs is observed for the FET based on the P3HT single crystal with the $\pi-\pi$ stacking direction perpendicular to the length axis of the crystal (i.e., current flow direction). The mobility showed feeble dependence on surface treatment of the FET device due

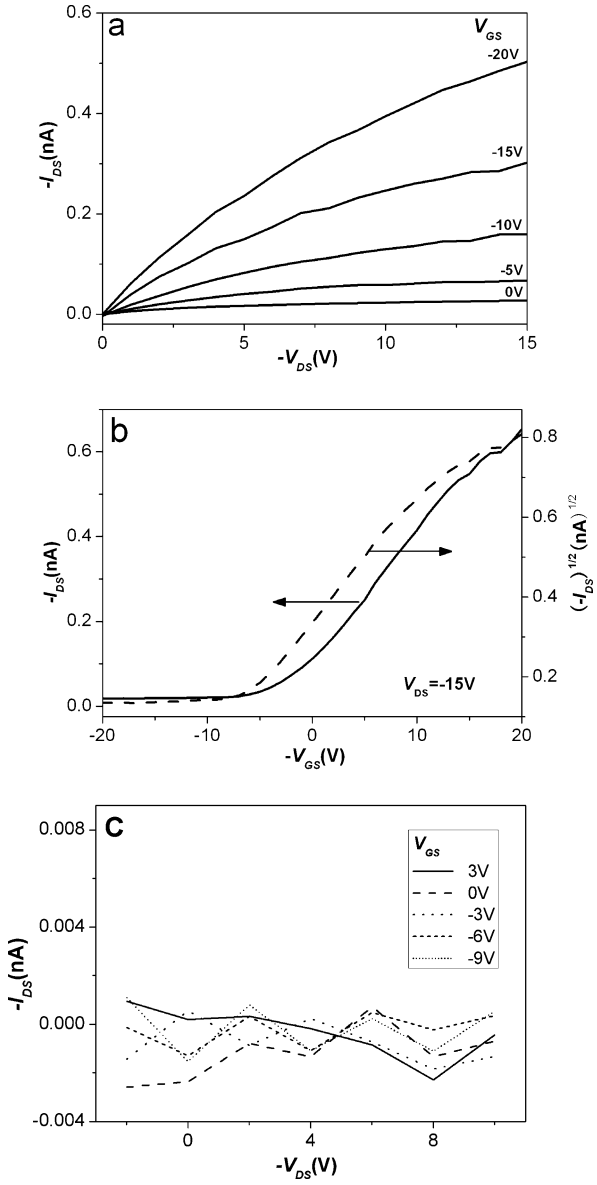

Figure 4. (a) Output characteristics of the FET based on a P3HT single crystal. (b) Transfer characteristics of the FET. The solid line manifests $-I_{DS}$ and the dashed line manifests $(-I_{DS})^{1/2}$. (c) Current−voltage characteristics of a device based on the THF-vapor-annealed film without P3HT single crystals.

to the highly crystalline structures of the P3HT single crystals.[71] No obvious difference was found in the mobility of P3HT single crystals with different heights, which indicates that the mobile channel region extends shallowly into the single crystals.[33]

It is well-known that the interchain charge hopping mainly determines the mobility of conducting polymers when the charge carriers migrate parallel to the substrate in FET.[10,39] During the hopping process, charges transport preferentially along the stacking axis of molecules through their overlapping of a π orbital. For the P3HT single crystal with the $\pi-\pi$ stacking direction parallel to the length axis of the crystal and main chain parallel to the substrate, interchain charge hopping is greatly facilitated due to the large overlap of a π orbital between molecules in-plane along the current flow direction.[3,35] Threfore, the FET based on the single crystal exhibited high current sensing and low voltage-gate modulation, and the authors declared that the mobility approached that of organic single crystals ($\approx 10^1$ cm^2/Vs),[35] as shown in Table 1.

For the P3HT single crystal with the $\pi-\pi$ stacking direction perpendicular to the current flow direction and the main chains parallel to the substrate in this work, the interchain charge hopping is greatly hampered. Therefore, the mobility ratio of the P3HT single crystals with the two different molecular conformations can be regarded as the in-plane anisotropy of electrical properties originating from $\pi-\pi$ stacking and main chain directions. The anisotropy is about 10^4, approaching the anisotropy of the conductivity parallel and perpendicular to the single crystal of graphite (10^4).[72]

The anisotropic properties of conjugated polymers have been studied, with many fruitful results obtained. The conductivity along the direction parallel to the film surface was much higher than that perpendicular to the film surface in solution-cast P3HT film, and the anisotropy was 953.[73] However, due to the inconvenient different device sets for measurement of electrical properties parallel and perpendicular to the film surface, the in-plane anisotropic properties that can be characterized rather conveniently are studied in most cases. The common polycrystalline film often showed in-plane isotropy, which can be obtained by mechanical stretching alignment, a friction-transfer technique, and so on.[74,75]

After the above-mentioned alignment treatment, the conjugated polymers are packed with $\pi-\pi$ stacking directions perpendicular; the main chains, parallel to the alignment direction. A higher mobility was obtained if the current flow was parallel to the alignment direction, and lower values were observed for orthogonal device orientation and the PL and electroluminescence (EL) polarized mainly in the alignment direction.[31,70,74,75]

In the friction-transferred film FET, the in-plane anisotropy of mobility reached up to 20 in P3HT and 8 in poly(3-dodecylthiophene) (P3DDT).[31,76] The friction-transferred P3ATs (including P3HT, P3OT, P3DT, and P3DDT) film exhibited anisotropic optical properties with a dichroic ratio more than 10.[75] In addition to P3ATs, another conjugated polymer also exhibited similar in-plane anisotropic properties with alignment treatment.[74,77] The in-plane anisotropy of the mobility parallel and perpendicular to the alignment direction of poly-9,9′-dioctylfluorene-*co*-bithiophene was 8 through chain alignment in a liquid crystalline phase, and the corresponding dichroic ratio was ∼10.[77] Compared with the in-plane anisotropic electrical properties of the P3HT single crystals originating from the $\pi-\pi$ stacking and main chain directions, the in-plane anisotropic electrical properties of the aligned film originating from the main chain and alkyl side chain directions are relatively low. These results indicate that although the better structural order in the single crystals may contribute to the higher anisotropy, the anisotropic electrical properties of conjugated polymers are dominated mainly by the molecular conformations.[32,74,78]

When the carriers migrate parallel to the substrate in FET, the charge transport of P3AT is determined mainly by interchain hopping, and the hole mobility is expected to decrease monotonically with increased side chain length due to the dilution effect of the insulating alkyl chains.[2,10,39−41] However, the reported mobility sequence of P3ATs with different alkyl side chain lengths showed different and even opposite results.[7,8,42,43] In some reports, the FET based on P3BT showed the highest mobility, and the monotonically decreased mobility with the increase of alkyl chain length was attributed to the "dilution effect" of the alkyl side chains.[79,80] In another case, it was observed that the mobility increased an order of magnitude from P3BT to P3HT and then decreased by almost 2 orders of magnitude to P3OT and decreased further to P3DT and P3DDT.

TABLE 1: Single Crystals of P3HT and P3OT with Different Molecular Conformations

sample	single crystal preparation conditions	orientation of length axis of crystal to $\pi-\pi$ stacking	mobility[a] (cm^2/Vs)
P3HT	THF vapor annealing (this work)	perpendicular	1.57×10^{-3}
	controlling solvent evaporation (ref 35)	parallel	≈ 10[b]
P3OT	THF vapor annealing (ref 37)	perpendicular	1.54×10^{-4}
	controlling solvent evaporation (this work)	parallel	0.62

[a] The mobility is obtained in the saturation regime from the FET based on the single crystals, and the current flow direction is along the length axis of the crystal. [b] The authors declared that the mobility of P3HT single crystals approached that of organic single crystals ($\approx 10^1$ cm^2/Vs).

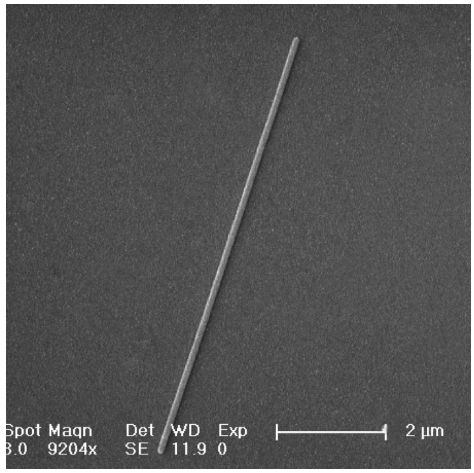

Figure 5. SEM image of a typical P3OT single crystal obtained by controlling solvent evaporation.

The mobility as a function of alkyl chain length with a peak at hexyl side chain was explained by the suggestion that mobility was a function of not only the alkyl chain length but also other morphological variables, such as the degree of crystallinity, crystallite size, etc.[42]

For the I_2-doped P3ATs, the conductivity sequence was PDDT > POT > PHT > PBT.[7] In single crystals of P3ATs with the same molecular conformation, the morphological variables and impurities are negligible, and the difference in mobility is caused by the alkyl side chain length. For single crystals of P3HT and P3OT with the $\pi-\pi$ stacking direction perpendicular to the length axis of the crystal, the mobility of P3HT is almost 1 order of magnitude higher than that of P3OT due to the shorter alkyl side chains (seen in Table 1). These results have demonstrated that the alkyl side chains play the role of a barrier to the carrier migration between the π-conjugated polymer chains.[37,40,41,43]

3.2. P3OT Single Crystals Obtained by Controlling Solvent Evaporation. ***3.2.1. Morphology and Structure Analysis of P3OT Single Crystals.*** Different from the needlelike single crystals of P3HT and P3OT obtained by THF vapor annealing,[37] the single crystals of P3OT obtained by controlling solvent evaporation are rodlike crystals with a length of 3−50 μm and a width of 150−800 nm. The SEM image of a typical P3OT single crystal is shown in Figure 5; the optical and SEM images of the crystals with different sizes are shown in Supporting Information Figures S6 and S7, respectively. The crystals possess a height of several hundred nanometers; the detailed AFM height images of a typical P3OT single crystal are shown in Supporting Information Figure S8.

The crystal structure and molecular orientation of the P3OT single crystals obtained by controlling solvent evaporation are revealed by XRD and SAED analysis. Polymorphism has been observed in P3OTs: the *a* axis about 20.9 Å is assigned as phase 1, and the *a* axis about 14.5 Å is assigned as phase 2.[12,55,57] The out-of-plane XRD profiles of the P3OT single crystals grown on a silicon wafer are shown in Figure 6a, and an interlayer *d*-spacing of 20.42 Å with a series of *h*00 reflections as 100, 200, and 300 are observed. According to the calculations from the ideal model, the *a* axis is 21.7 Å for POT, and the experimental value deviates from the calculated value by 1.3 Å, indicating a minimal interdigitation of alkyl side chains in phase 1.[12] The XRD results indicate that the *a* axis is oriented perpendicular to the crystal surface with the *bc* plane of the crystal on the substrate. The TEM image of part of a crystal is shown in Figure 6b, and the SAED obtained perpendicular to the length axis of the crystal is manifested in Figure 6c. The

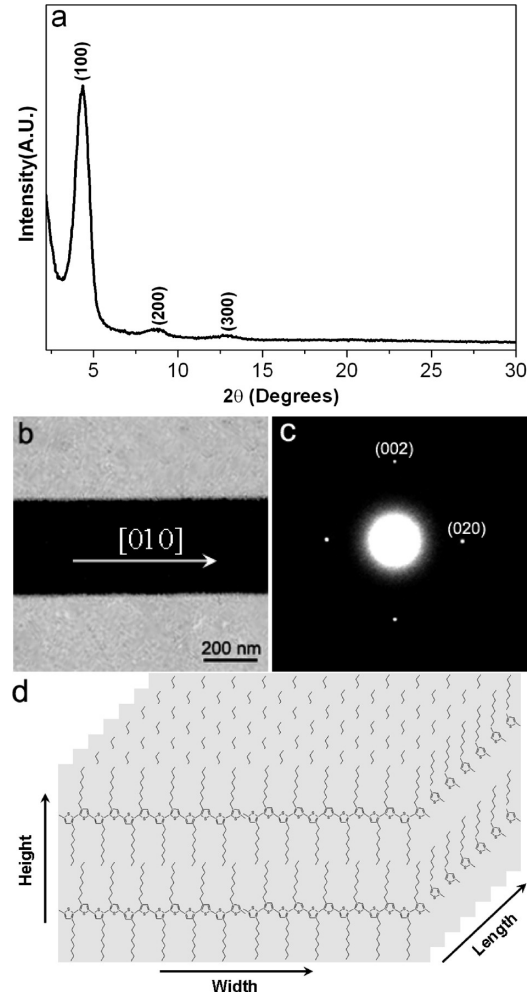

Figure 6. Structure and molecular orientation of the P3OT single crystals. (a) XRD profiles of P3OT crystals grown on a silicon wafer. (b) TEM image of part of a single crystal. (c) SAED pattern obtained perpendicular to the length axis of the crystal. (d) Schematic illustrations for the assembly of the extended polymer chains in the crystal. For clarity, the relative dimensions are not drawn to scale.

SAED results exhibited a repeating unit of 7.42 Å along the polymer chain direction and a repeating unit of 8.38 Å along the $\pi-\pi$ stacking direction.

For P3OT in phase 1, the $\pi-\pi$ stacking distance has been reported to be about 3.7−3.9 Å in some cases, and a larger distance of 4.85 Å was even reported.[12,55] For P3OT in phase 2, values such as 4.47, 4.7, or 5.5 Å are reported.[53−55] Since the $\pi-\pi$ stacking distances of P3ATs with different alkyl side chains are almost identical under the same conditions, we can speculate that the structure of P3OT that suits the energetically most stable form possesses a $\pi-\pi$ stacking distance of ∼4.14 Å, similar to that of P3HT and P3OT.[12,50,55,56] The observed $\pi-\pi$ stacking distance of 4.19 Å for the P3OT single crystal almost coincides with 4.14 Å, but it obviously deviates from those of phase 2. Thus, it can be inferred that the phase 1structure with the corresponding cell parameters is the thermostable state for P3OT single crystals under these conditions. It is considered that the high molecular weight of 51k and high regioregularity of 98.5% of the P3OT sample together with the crystallization conditions favored the formation of phase 1 rather than phase 2. The 0*kl* reflections in SAED confirmed the (100) projection from XRD results, and the length axis of the single crystal is observed to be along the $\pi-\pi$ stacking direction.[16,37,50,54] Thus, it is concluded that in the P3OT single crystals, the extended polymer chains are packed with the $\pi-\pi$ stacking direction parallel to the length axis of the crystal and the main chains parallel to the substrate. The schematic illustration for the assembly of molecules in the single crystals is shown in Figure 6d.

3.2.2. Growth of P3OT Single Crystals. As we see, solvent evaporation is a strong, highly directional field. During the solution-crystallization process, when the solvent evaporated at a very slow speed, the molecules could diffuse over a certain distance, remove volatile solvent, exclude defects, and optimize chain packing.[81−83] As a conjugated polymer, the $\pi-\pi$ intermolecular interactions play an important role during the crystallization of P3ATs, and it is proved that in solution-cast P3AT films, the growth of the whisker crystals is dominated by $\pi-\pi$ interactions.[23,59] Similarly, the growth of P3HT single crystals is dominated by $\pi-\pi$ interactions, and the molecules are packed with the $\pi-\pi$ stacking direction parallel to the length axis of the crystals when the solvent evaporates slowly.[35] In this work, the solvent vapor pressure generated by the precast solvent together with the covered lid lead to the slow evaporation of the solvent from the P3OT solution deposited on the substrate. Thus, single crystals of P3OT with $\pi-\pi$ stacking direction parallel to the length axis of the rod-like crystal and main chains parallel to the substrate are obtained. Unlike the P3HT single crystals obtained by THF vapor annealing, the $\pi-\pi$ interactions mainly determined the growth and the corresponding molecular conformation when the P3OT single crystals were obtained by controlling solvent evaporation.

3.2.3. Electrical Properties of P3OT Single Crystals. The typical output and transfer characteristics of the FET based on the P3OT single crystal are shown in Figure 7. Figure 7a shows the I_{DS} curves versus V_{DS} with differentV_{GS}, and Figure 7b shows the $-I_{DS}$ and $(-I_{DS})^{1/2}$ curves versus $-V_{GS}$. As shown in Figure 7c, no channel conductance or gate dependence is detected in regions without P3OT single crystals, which means that the gate modulation is attributed to the P3OT single crystals. The surface treatment exerted little influence on the mobility due to the highly crystalline nature of the single crystals,[71] and the height of the crystals showed negligible effects on the mobility due to the shallow extension of mobile channel regions into the single

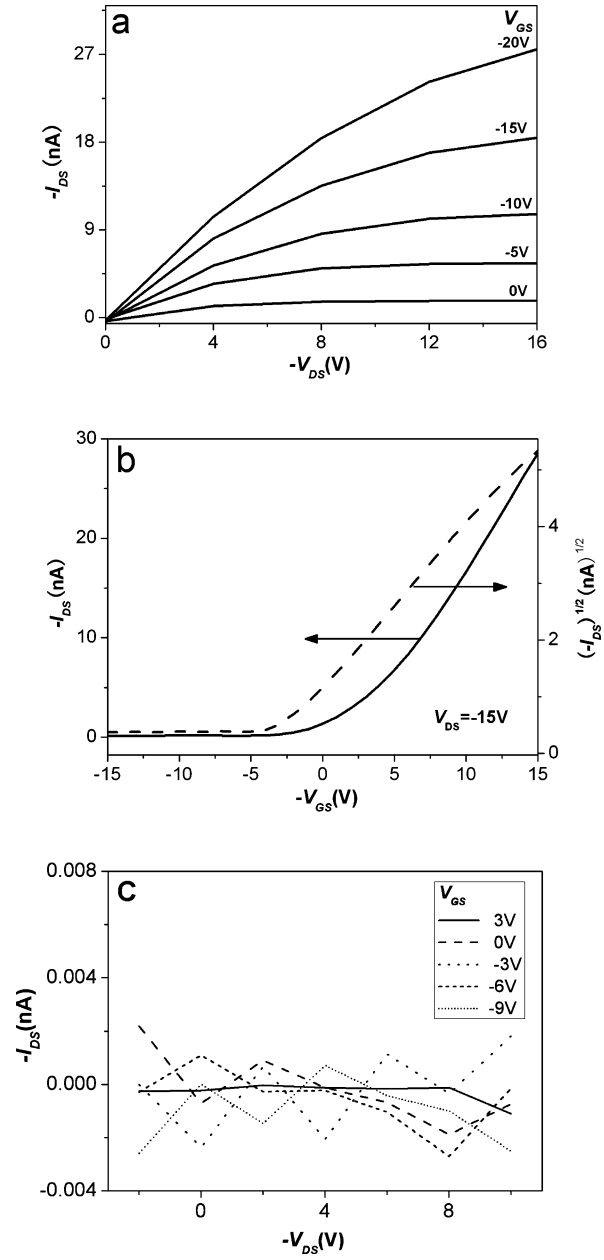

Figure 7. (a) Output characteristics of the FET based on a P3OT single crystal. (b) Transfer characteristics of the FET. The solid line manifests $-I_{DS}$, and the dashed line manifests $(-I_{DS})^{1/2}$. (c) Current−voltage characteristics of a device without P3OT single crystals.

crystals. An effective mobility of 0.62 cm^2/Vs is obtained for the P3OT single crystal.

The regioregular poly(3-(2-(*s*)-methylbutyl)thiophene) with a $\pi-\pi$ stacking distance of 4.3 Å showed a mobility on the order of 10^{-3} cm^2/Vs at film, which indicated that efficient overlapping of a π orbital can occur within a distance of 4.3 Å,[84] and the P3OT thin films showed a similar mobility.[42,79,85] The particular molecular conformation with the $\pi-\pi$ stacking direction parallel to the current flow direction and the main chains parallel to the substrate in the highly perfect ordered single crystals leads to much higher mobility, as expected. As shown in Table 1, a P3OT single crystal with the $\pi-\pi$ stacking direction perpendicular to the current flow direction and main chain parallel to the substrate showed a mobility of 1.54×10^{-4} cm^2/Vs. Therefore, the in-plane anisotropy of P3OT single crystals stemming from the $\pi-\pi$ stacking and the main chain direction is $\sim 4 \times 10^3$, much higher than the in-plane anisotropy

from the main chain and alkyl chain directions in the friction-transferred film.[31,75,76]

When the P3HT and P3OT single crystals are of the same molecular conformation with the $\pi-\pi$ stacking direction parallel to the length axis of the crystal and main chains parallel to the substrate, the mobility of the P3HT single crystals is about 20 times higher than that of P3OT, and the shorter alkyl side chain length of P3HT, as compared with P3OT, is assumed to cause the higher mobility. These results further confirmed the above-mentioned conclusions that the anisotropic electrical properties of conjugated polymers are determined mainly by molecular conformations, the charges transport preferentially along the $\pi-\pi$ stacking direction, and the alkyl side chains function as barriers to carrier migration between P3ATs. The processes to prepare P3HT and P3OT single crystals, the molecular conformations, and the corresponding electrical properties of the single crystals are summarized in Table 1.

4. Conclusions

We have demonstrated that single crystals of P3HT with the $\pi-\pi$ stacking direction perpendicular to the length axis of the crystals and main chains parallel to the substrate can be obtained by THF vapor annealing, and the crystals possess the mobility of 1.57×10^{-3} cm^2/Vs. Single crystals of P3OT with the $\pi-\pi$ stacking direction parallel to the length axis of the crystal and main chains parallel to the substrate can be obtained by controlling solvent evaporation; the mobility is 0.62 cm^2/Vs. High anisotropy of electrical properties is observed in the single crystals, and these results manifested that the device performance is crucially determined by the molecular conformation, with the charges transporting preferentially along the $\pi-\pi$ stacking direction. The higher mobility of P3HT single crystals than that of P3OT with the same molecular conformation indicated that the alkyl side chains function as barriers to carrier migration between P3AT polymers.

These results point to the importance of understanding and controlling the molecular conformation in electron devices based on P3ATs. They may stimulate further study of the intrinsic charge transport mechanism of conducting polymers and shed light on the side chain length dependence of charge carrier mobility in other side-chain-substituted π-conjugated polymers.

Acknowledgment. The authors thank Prof. Wenping Hu and Prof. Yunqi Liu, Dr. Yugeng Wen, and Yajie Zhang (Institute of Chemistry, Chinese Academy of Science) for assistance in the fabrication of FET and the National Key Micrometer/Nanometer Processing Laboratory for the supply of silicon wafers. This work is supported by the National Natural Science Foundation of China (20774095).

Supporting Information Available: The optical and SEM images of the needlelike P3HT single crystals obtained by THF vapor annealing are shown in Figure S1 and Figure S2, respectively. The detailed AFM height image of a fully grown P3HT single crystal is shown in Figure S3, and the AFM height image of a P3HT crystal with a length of $\sim$10 μm is shown in Figure S4. The schematic illustration for the configuration of FET base on the single crystals and the SEM image of the crystals measured are shown in Figure S5. The optical and SEM images of the rodlike P3OT single crystals obtained by controlling solvent evaporation are shown in Figure S6 and Figure S7, respectively. The detailed AFM height image of a P3OT single crystal is shown in Figure S8. This material is available free of charge via the Internet at http://pubs.acs.org.

References and Notes

(1) Patil, A. O.; Heeger, A. J.; Wudl, F. *Chem. Rev.* **1988**, *88*, 183.
(2) Chen, T. A.; Wu, X.; Rieke, R. D. *J. Am. Chem. Soc.* **1995**, *117*, 233.
(3) Fichou, D. *Handbook of Oligo- and Polythiophenes*, 1st. ed.; Wiley: Weinheim, 1999.
(4) Wang, G.; Swensen, J.; Moses, D.; Heeger, A. J. *Appl. Phys. Lett.* **2003**, *93*, 6137.
(5) Sirringhaus, H.; Tessler, N.; Friend, R. H. *Science* **1998**, *280*, 1741.
(6) Yang, X.; Loos, J.; Veenstra, S. C.; Verhees, W. J. H.; Wienk, M. M.; Kroon, J. M.; Michels, M. A. J.; Janssen, R. A. J. *Nano Lett.* **2005**, *5*, 579.
(7) McCullough, R. D.; Nagle, S. T.; Williams, S. P.; Lowe, R. D.; Jayaramant, M. *J. Am. Chem. Soc.* **1993**, *115*, 4910.
(8) Bao, Z.; Feng, Y.; Dodabalapur, A.; Raju, V. R.; Lovinger, A. J. *Chem. Mater.* **1997**, *9*, 1299.
(9) Sirringhaus, H.; Brown, P. J.; Friend, R. H.; Nielsen, M. M.; Bechgaard, K.; Langeveld-Voss, B. M. W.; Spiering, A. J. H.; Janssen, R. A. J.; Meijer, E. W.; Herwig, P.; de Leeuw, D. M. *Nature* **1999**, *401*, 685.
(10) Schön, J. H.; Dodabalapur, A.; Bao, Z.; Kloc, C.; Schenker, O.; Batlogg, B. *Nature* **2001**, *410*, 189.
(11) Ayzner, A. L.; Wanger, D. D.; Tassone, C. J.; Tolbert, S. H.; Schwartz, B. J. *J. Phys. Chem. C* **2008**, *112*, 18711.
(12) Chen, S. A.; Ni, J. M. *Macromolecules* **1992**, *25*, 6081.
(13) Huynh, W. U.; Dittmer, J. J.; Alivisatos, P. *Science* **2002**, *295*, 2425.
(14) Goh, C.; Kline, R. J.; McGehee, M. D.; Kadnikova, E. N.; Fréchet, J. M. J. *Appl. Phys. Lett.* **2005**, *86*, 122110.
(15) Brinkmann, M.; Rannou, P. *Adv. Funct. Mater.* **2007**, *17*, 101.
(16) Prosa, T. J.; Winokur, M. J.; Moulton, J.; Smith, P.; Heeger, A. J. *Macromolecules* **1992**, *25*, 4364.
(17) Kline, R. J.; McGehee, M. D.; Kadnikova, E. N.; Liu, J.; Frechet, J. M. J. *Adv. Mater.* **2003**, *15*, 1519.
(18) Zen, A.; Saphiannikova, M.; Neher, D.; Grenzer, J.; Grigorian, S.; Pietsch, U.; Asawapirom, U.; Janietź, S.; Scherf, U.; Lieberwirth, I.; Wegner, G. *Macromolecules* **2006**, *39*, 2162.
(19) Bao, A.; Dodabalapur, A.; Lovinger, A. J. *Appl. Phys. Lett.* **1996**, *69*, 4108.
(20) Janzen, D. E.; Burand, M. W.; Ewbank, P. C.; Pappenfus, T. M.; Higuchi, H.; da Silva Filho, D. A.; Young, V. G.; Brédas, J. L.; Mann, K. R. *J. Am. Chem. Soc.* **2004**, *126*, 15295.
(21) Collard, D. M.; Fox, M. A. *J. Am. Chem. Soc.* **1991**, *113*, 9414.
(22) Lambert, T.; Ferraris, J. P. *J. Chem. Soc., Chem. Commun.* **1991**, *11*, 752.
(23) Zhang, R.; Li, B.; Iovu, M. C.; Jeffries-EL, M.; Sauvé, G.; Cooper, J.; Jia, S.; Tristram-Nagle, S.; Smilgies, D. M.; Lambeth, D. N.; McCullough, R. D.; Kowalewski, T. *J. Am. Chem. Soc.* **2006**, *128*, 3480.
(24) Li, G.; Shrotriya, V.; Yao, Y.; Huang, J.; Yang, Y. *J. Mater. Chem.* **2007**, *17*, 3126.
(25) Reese, C.; Bao, Z. *Mater. Today* **2007**, *10*, 20.
(26) Zhang, M.; Hu, Z.; He, T. *J. Phys. Chem. B* **2004**, *108*, 19198.
(27) Lee, J. Y.; Roth, S.; Park, Y. W. *Appl. Phys. Lett.* **2006**, *88*, 252106.
(28) Zeis, R.; Besnard, C.; Siegrist, T.; Schlockermann, C.; Chi, X.; Kloc, C. *Chem. Mater.* **2006**, *18*, 244.
(29) Gao, Z. Q.; Zhou, L.; Huang, H. *Thin Solid Films* **1999**, *347*, 146.
(30) Amundson, K. R.; Sapjeta, B. J.; Lovinger, A. J.; Bao, Z. N. *Thin Solid Films* **2002**, *414*, 143.
(31) Nagamatsu, S.; Tanigaki, N.; Yoshida, Y.; Takashima, W.; Yase, K.; Kaneto, K. *Synth. Met.* **2003**, *137*, 923.
(32) Garnier, F.; Yassar, A.; Hajlaoui, R.; Horowitz, G.; Deloffre, F.; Servet, B.; Ries, S.; Alnot, P. *J. Am. Chem. Soc.* **1993**, *115*, 8716.
(33) Kim, D. H.; Park, Y. D.; Jang, Y. S.; Yang, H. C.; Kim, Y. H.; Han, J. I.; Moon, D. G.; Park, S.; Chang, T.; Chang, C.; Joo, M.; Ryu, C. Y.; Cho, K. *Adv. Funct. Mater.* **2005**, *15*, 77.
(34) Zen, A.; Pflaum, J.; Hirschmann, S.; Zhuang, W.; Jaiser, F.; Asawapirom, U.; Rabe, J. P.; Scherf, U.; Neher, D. *Adv. Funct. Mater.* **2004**, *14*, 757.
(35) Kim, D. H.; Han, J. T.; Park, Y. D.; Jang, Y.; Cho, J. H.; Hwang, M.; Cho, K. *Adv. Mater.* **2006**, *18*, 719.
(36) Ma, Z.; Geng, Y.; Yan, D. *Polymer* **2007**, *48*, 31.
(37) Xiao, X.; Hu, Z.; Wang, Z.; He, T. *J. Phys. Chem. B* **2009**, *113*, 14604.
(38) Schoonveld, W. A.; Vrijmoeth, J.; Klapwijk, T. M. *Appl. Phys. Lett.* **1998**, *73*, 3884.
(39) Basescu, N.; Liu, Z. X.; Moses, D.; Heeger, A. J.; Naarmann, H.; Theophilou, N. *Nature* **1987**, *327*, 403.
(40) Moulton, J.; Smith, P. *Polymer* **1992**, *33*, 2340.
(41) Aasmundtveit, K. E.; Samuelsen, E. J.; Guldstein, M.; Steinsland, C.; Flornes, O.; Fagermo, C.; Seeberg, T. M.; Pettersson, L. A. A.; Inganäs, O.; Feidenhans'l, R.; Ferrer, S. *Macromolecules* **2000**, *33*, 3120.
(42) Babel, A.; Jenekhe, S. A. *Syn. Met.* **2005**, *148*, 169.

(43) Zen, A.; Saphiannikova, M.; Neher, D.; Asawapirom, U.; Scherf, U. *Chem. Mater.* **2005**, *17*, 781.
(44) Gránásy, L.; Pusztai, T.; Börzsönyi, T.; Warren, J. A.; Douglas, J. F. *Nat. Mater.* **2004**, *3*, 645.
(45) Yamashita, Y.; Kato, Y.; Endo, S.; Kimura, K. *Makromol. Chem., Rapid Commun.* **1988**, *9*, 687.
(46) Taesler, C.; Petermann, J.; Kricheldorf, H. R.; Schwarz, G. *Makromol. Chem.* **1991**, *192*, 2255.
(47) Iguchi, M.; Murase, I. *J. Cryst. Growth* **1974**, *24/25*, 596.
(48) Causin, V.; Marega, C.; Valentini, A. M. L.; Kenny, J. M. *Macromolecules* **2005**, *38*, 409.
(49) Corish, J.; Morton-Blake, D. A.; Beniere, F.; Lantoine, M. *J. Chem. Soc., Faraday Trans.* **1996**, *92*, 671.
(50) Tashiro, K.; Kobayashi, M.; Kawai, T.; Yoshino, K. *Polymer* **1997**, *38*, 2867.
(51) Tashiro, K.; Ono, K.; Minagawa, Y.; Kobayashi, M.; Kawai, T.; Yoshino, K. *J. Polym. Sci., Part B: Polym. Phys.* **1991**, *29*, 1223.
(52) Joshi, S.; Grigorian, S.; Pietsch, U. *Phys. Status Solidi* **2008**, *205*, 488.
(53) Meille, S. V.; Romita, V.; Caronna, T.; Lovinger, A. J.; Catellani, M.; Belobrzeckaja, L. *Macromolecules* **1997**, *30*, 7898.
(54) Prosa, T. J.; Winokur, M. J.; McCullough, R. D. *Macromolecules* **1996**, *29*, 3654.
(55) Bolognesi, A.; Porzio, W.; Provasoli, A.; Botta, C.; Comotti, A.; Sozzani, P.; Simonutti, R. *Macromol. Chem. Phys.* **2001**, *202*, 2586.
(56) Yang, C.; Orfino, F. P.; Holdcroft, S. *Macromolecules* **1996**, *29*, 6510.
(57) Tashiro, K.; Minagawa, Y.; Kobayashi, M.; Morita, S.; Kawai, T.; Yoshino, K. *Synth. Met.* **1993**, *55*, 321.
(58) Lu, G.; Li, L.; Yang, X. *Adv. Mater.* **2007**, *19*, 3594.
(59) Bolognesi, A.; Catellani, M.; Destri, S.; Porzio, W. *Makromol. Chem., Rapid Commun.* **1991**, *12*, 9.
(60) Kimura, K.; Yamashita, Y. *Polymer* **1994**, *35*, 3311.
(61) Park, J. H.; Kim, J. S.; Lee, J. H.; Lee, W. H.; Cho, K. *J. Phys. Chem. C* **2009**, *113*, 17579.
(62) Zhao, Y.; Guo, X.; Xie, Z.; Qu, Y.; Geng, Y.; Wang, L. *J. Appl. Polym. Sci.* **2009**, *111*, 1799.
(63) Gregg, B. A. *J. Phys. Chem.* **1996**, *100*, 852.
(64) Dickey, K. C.; Anthony, J. E.; Loo, Y. L. *Adv. Mater.* **2006**, *18*, 1721.
(65) Mascaro, D. J.; Thompson, M. E.; Smith, H. I.; Bulović, V. *Org. Electron.* **2005**, *6*, 211.
(66) Law, K. Y. *Chem. Rev.* **1993**, *93*, 449.
(67) Conboy, J. C.; Olson, E. J. C.; Adams, D. M.; Kerimo, J.; Zaban, A.; Gregg, B. A.; Barbara, P. F. *J. Phys. Chem. B* **1998**, *102*, 4516.
(68) Dundon, M. L. *J. Am. Chem. Soc.* **1923**, *45*, 2658.
(69) Ihn, K. J.; Moulton, J.; Smith, P. *J. Polym. Sci., Part B: Polym. Phys.* **1993**, *31*, 735.
(70) Dyreklev, P.; Berggren, M.; Inganäs, O.; Andersson, M. R.; Wennerstrom, O.; Hjertberg, T. *Adv. Mater.* **1994**, *7*, 43.
(71) Liu, J.; Arif, M.; Zou, J.; Khondaker, S. I.; Zhai, L. *Macromolecules* **2009**, *42*, 9390.
(72) Dutta, A. K. *Phys. Rev.* **1953**, *90*, 187.
(73) Liu, C.; Oshima, K.; Shimomura, M.; Miyauchi, S. *Synth. Met.* **2006**, *156*, 1362.
(74) Bolognesi, A.; Botta, C.; Martinelli, M.; Porzio, W. *Org. Electron.* **2000**, *1*, 27.
(75) Nagamatsu, S.; Takashima, W.; Kaneto, K.; Yoshida, Y.; Tanigaki, N.; Yase, K.; Omote, K. *Macromolecules* **2003**, *36*, 5252.
(76) Nagamatsu, S.; Takashima, W.; Kaneto, K.; Yoshida, Y.; Tanigaki, N.; Yase, K. *Appl. Phys. Lett.* **2004**, *84*, 4608.
(77) Sirringhaus, H.; Wilson, R. J.; Friend, R. H.; Inbasekaran, M.; Wu, W.; Woo, E. P.; Grell, M.; Bradley, D. D. C. *Appl. Phys. Lett.* **2000**, *77*, 406.
(78) Chen, X. L.; Lovinger, A. J.; Bao, Z.; Sapjeta, J. *Chem. Mater.* **2001**, *13*, 1341.
(79) Park, Y. D.; Kim, D. H.; Jang, Y.; Cho, J. H.; Hwang, M.; Lee, H. S.; Lim, J. A.; Cho, K. *Org. Electron.* **2006**, *7*, 514.
(80) Kaneto, K.; Lim, W. Y.; Takashima, W.; Endo, T.; Rikukawa, M. *Jpn. J. Appl. Phys.* **2000**, *39*, L872.
(81) Wunderlich, B. Crystal structure, morphology, defects. *Macromolecular Physics*; Academic Press: New York, 1973; Vol. 1; p 178.
(82) Kim, S. H.; Misner, M. J.; Xu, T.; Kimura, M.; Russell, T. P. *Adv. Mater.* **2004**, *16*, 226.
(83) Hu, Z. J.; Zhang, F. J.; Huang, H. Y.; Zhang, M. L.; He, T. B. *Macromolecules* **2004**, *37*, 3310.
(84) Bao, Z.; Lovinger, A. J. *Chem. Mater.* **1999**, *11*, 2607.
(85) Lutsyk, P.; Janus, K.; Mikolajczyk, M.; Sworakowski, J.; Boratynski, B.; Tlaczala, M. *Org. Electron.* **2010**, *11*, 490.

JP911525D